Developmental Cell
Short Article

Independent Genomic Control of Neuronal Number across Retinal Cell Types

Patrick W. Keeley,[1,2] Irene E. Whitney,[1,2] Nils R. Madsen,[1] Ace J. St. John,[1] Sarra Borhanian,[1,2] Stephanie A. Leong,[1,2] Robert W. Williams,[4,5] and Benjamin E. Reese[1,3,*]
[1]Neuroscience Research Institute, University of California, Santa Barbara, Santa Barbara, CA 93106, USA
[2]Department of Molecular, Cellular, and Developmental Biology, University of California, Santa Barbara, Santa Barbara, CA 93106, USA
[3]Department of Psychological and Brain Sciences, University of California, Santa Barbara, Santa Barbara, CA 93106, USA
[4]Center of Genomics and Bioinformatics, University of Tennessee Health Science Center, Memphis, TN 38120, USA
[5]Department of Anatomy and Neurobiology, University of Tennessee Health Science Center, Memphis, TN 38120, USA
*Correspondence: breese@psych.ucsb.edu
http://dx.doi.org/10.1016/j.devcel.2014.05.003

SUMMARY

The sizes of different neuronal populations within the CNS are precisely controlled, but whether neuronal number is coordinated between cell types is unknown. We examined the covariance structure of 12 different retinal cell types across 30 genetically distinct lines of mice, finding minimal covariation when comparing synaptically connected or developmentally related cell types. Variation mapped to one or more genomic loci for each cell type, but rarely were these shared, indicating minimal genetic coregulation of final number. Multiple genes, therefore, participate in the specification of the size of every population of retinal neuron, yet genetic variants work largely independent of one another during development to modulate those numbers, yielding substantial variability in the convergence ratios between pre- and postsynaptic populations. Density-dependent cellular interactions in the outer plexiform layer overcome this variability to ensure the formation of neuronal circuits that maintain constant retinal coverage and complete afferent sampling.

INTRODUCTION

Neuron number is determined by numerous developmental processes, including proliferation, fate assignment, differentiation, and apoptosis (Bassett and Wallace, 2012; Lui et al., 2011; Southwell et al., 2012). Although the size of a neuronal population in different parts of the CNS is known to be modulated genetically, the extent to which cell populations within a structure covary has been unexplored. The retina is an ideal structure for studying the precision of cellular demographics in the CNS, because most populations of neuron are confined to a single layer within a well-defined area, permitting accurate quantification. Variation in the number of different types of synaptically connected neurons, furthermore, should have functional consequences because convergence and divergence ratios define the receptive field organization and response properties of postsynaptic neurons (Balasubramanian and Sterling, 2009; Xiong and Finlay, 1996). Because gene variants may bias fate choices within neuronal precursors, or modulate rates of apoptosis of interconnected cells (Whitney et al., 2009, 2011a), correlations (negative or positive) between developmentally and functionally related cell types are to be expected.

To gain insight into the covariance structure of multiple neuronal populations, we quantified 12 different populations of neurons in the retina (Figures 1A and 1B) across a genetically diverse set of 30 lines of mice. These included two common inbred laboratory strains, the genomes of which having been fully sequenced (C57BL/6J and A/J), their isogenic F1 offspring, and 26 recombinant inbred (RI) strains (the AXB/BXA strain set). As each of these RI strains has been genotyped at high density using single-nucleotide polymorphisms and microsatellite markers (Williams et al., 2001), we were able to map genomic sources of heritable variation in neuronal number to chromosomal positions (loci) and to examine the degree of joint or independent genetic control over the size of these 12 populations.

RESULTS

Cell Number Is Precisely Specified within a Strain

The populations of retinal neurons sampled included rod and cone photoreceptor cells, horizontal cells, four different types of bipolar cell, and five different types of amacrine cell (Figures 1A and 1B). Neuronal number showed low variability within each strain, for every cell type examined (Table S1 available online). The average coefficient of variation (CoV) across all strains for each cell type (Figure 1C) ranged from 0.030 (for the vesicular glutamate transporter 3 [VGluT3] amacrine cells) to 0.065 (for the type 4 cone bipolar cells), and there was no correlation between average CoV and the size of the population across the 12 cell types ($r = -0.26$; $p = 0.41$). This modest and consistent level of within-strain variation demonstrates that the sampling methods for these cells were reliable despite large variation in the proportion of retinal area sampled: the entire retina was sampled for the dopaminergic amacrine cells (being the sparsest of all cell types sampled), whereas less than one-tenth of 1% of retinal area was sampled in the case of the rod photoreceptors (the most numerous cell type). This accuracy by which the developing retina specifies neuron number is perhaps most remarkable when one considers the fact that the sizes of these populations differ by four orders of magnitude.

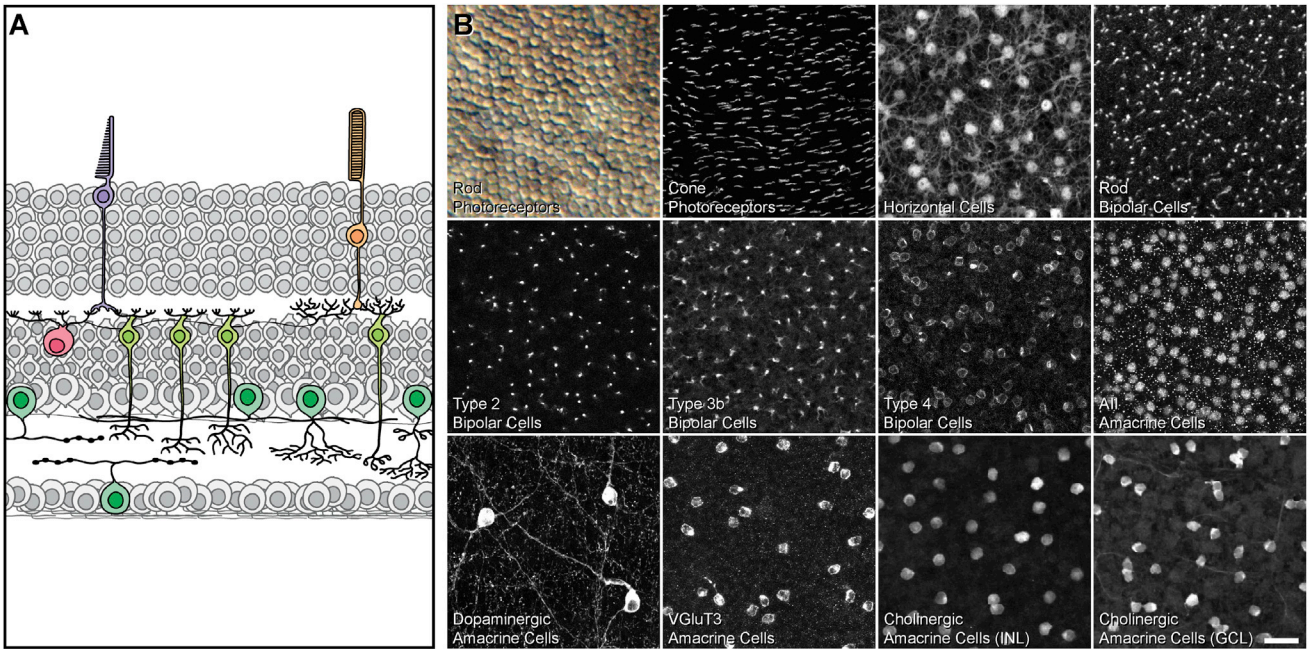

C

	Min	Max	% Increase	Average CoV	h^2	Largest QTL	LRS for Largest QTL	Additive effect	Magnitude of effect	Accession #
Rod	6,051,100	8,227,260	36	0.036	0.48	Chr 11: 5.226907 Mb	12.0	494,913 (*B*)	0.23	10268
Cone	116,158	204,419	76	0.061	0.67	Chr 10: 20.127244 Mb	14.7	21,946 (*B*)	0.25	10153
HC	9,884	18,942	92	0.034	0.89	Chr 13: 113.528364 Mb	18.1	2,490 (*B*)	0.28	10132
RBC	202,415	254,176	26	0.046	0.44	Chr 4: 132.410009 Mb	14.0	19,293 (*A*)	0.37	10202
CBC2	41,908	60,570	45	0.046	0.58	Chr 2: 3.803360 Mb	12.5	6,127 (*A*)	0.33	10181
CBC3b	50,243	80,469	60	0.050	0.64	Chr 6: 107.743813 Mb	14.4	8,607 (*A*)	0.29	10257
CBC4	29,351	50,260	71	0.065	0.69	Chr 18: 70.077348 Mb	16.7	7,491 (*A*)	0.36	10263
AII	57,141	86,557	51	0.046	0.74	Chr 11: 5.226907 Mb	14.6	11,640 (*B*)	0.40	10179
DA	160	637	298	0.045	0.87	Chr 7: 72.726203 Mb	15.2	149 (*B*)	0.31	10127
VGluT3	10,415	14,857	43	0.030	0.82	Chr 5: 144.381933 Mb	14.7	1,591 (*A*)	0.36	10262
ChAT INL	14,506	22,304	54	0.041	0.68	Chr 16: 6.548996 Mb	10.4	1,859 (*B*)	0.24	10131
ChAT GCL	12,434	18,414	48	0.040	0.63	-	-	-	-	10129

Figure 1. Conspicuous Strain Variation Exists for All Cell Types, from which Large-Effect QTL Can Be Mapped

(A) The 12 cell types examined shown in schematic cross-section of the retina.

(B) Images from whole-mount preparations showing those sampled cell types. The scale bar indicates 5 μm for the rod photoreceptors and 25 μm for the remaining cell types.

(C) Listed for each cell type is the range (min and max referring to the total number of cells present in the strain with the lowest and highest totals, respectively), the percentage increase from the lowest to the highest strain, and the average coefficient of variation across the strains; the estimated heritable component of that variation (h^2); the genomic locus (chromosome and Mb, respectively) and magnitude of the largest QTL detected for each cell type, expressed as the LRS of that QTL, and in cell number (the "additive effect"; *A* or *B* indicating the haplotype correlating with an increase in trait values at each locus); and the magnitude of that effect as a proportion of the range observed across the RI strains. Finally, the accession numbers for the data in GeneNetwork (http://www.genenetwork.org) are listed. Full details for each strain (including the mean, SE, CoV, and n) are provided in Table S1.

Large Variation in Cell Number Is Present between Strains

Such minimal variance in cell number within a strain is to be contrasted with the conspicuous variation between strains (Table S1). Rod photoreceptor number, for example, was lowest in the A/J strain, being 6,050,000 ± 169,000 cells (mean ± SEM, and hereafter), climbing to 8,230,000 ± 51,000 cells in the BXA12 RI strain, a 36% increase (Figure 3B). By contrast, VGluT3+ amacrine cell number was lowest in the BXA25 RI strain, being 10,400 ± 80 cells, reaching 14,900 ± 220 cells in BXA12, being a 43% increase (Figure 3A). Variation across strains was significant and sizable for every cell type (Figure 1C), in some cases approaching a 2- or 3-fold variation. Note as well that, for some cell types, the parental strains showed minimal difference in total number, yet substantial variation was present across the RI strain set (Table S1). We can estimate the magnitude of the genetic contribution controlling cell number by calculating the heritability (h^2) for each cell type (Hegmann and Possidente, 1981), being the proportion of the total variance across all mice that can be ascribed to an effect of strain (Figure 1C). For some cell types, nearly 90% of that variation among individual mice was due to an effect of genotype (e.g., horizontal cells, dopaminergic amacrine cells), whereas for others, heritability was only about one-half this value (e.g., rod photoreceptors,

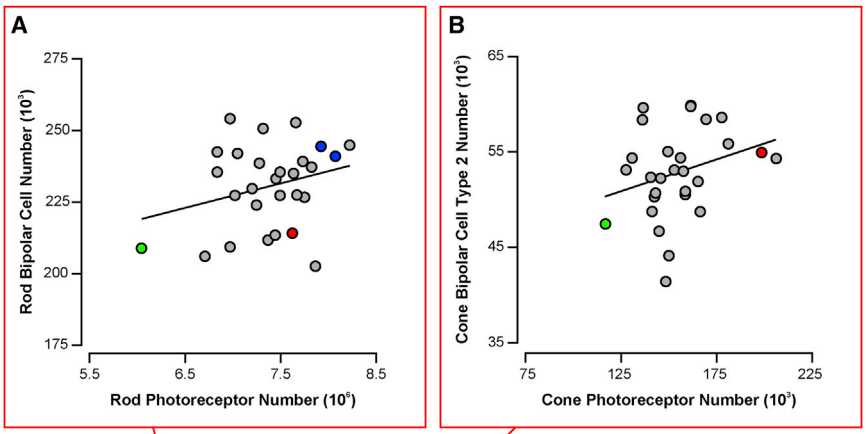

C

		Rod	Cone	HC	RBC	CBC2	CBC3b	CBC4	AII	DA	VGluT3	ChAT INL
Cone	*r* =	0.34										
HC		0.34	**0.43**									
RBC		0.24	0.13	0.10								
CBC2		0.34	0.28	0.09	**0.52**							
CBC3b		**0.43**	0.24	**0.53**	0.20	0.10						
CBC4		**0.57**	0.04	-0.11	-0.09	0.13	0.15					
AII		**0.48**	0.01	0.08	0.31	0.25	0.20	**0.40**				
DA		**0.38**	0.30	0.33	0.06	0.09	0.21	0.23	0.24			
VGluT3		**0.49**	0.14	0.17	**0.40**	**0.51**	0.27	0.23	**0.58**	0.28		
ChAT INL		0.30	0.11	0.08	**0.50**	0.31	0.09	0.25	0.09	0.11	0.08	
ChAT GCL		**0.50**	0.16	0.22	**0.40**	0.35	0.29	0.27	0.26	0.27	0.16	**0.81**

Figure 2. Minimal Covariation between Developmentally or Functionally Related Cell Types Is Present

(A and B) No significant correlation was detected between the number of rod (A) or cone (B) photoreceptors and the number of rod or type 2 cone bipolar cells, respectively. F1 strain data were not collected for cone photoreceptors (as indicated in Table S1), so the F1 strains are excluded in (B).

(C) The correlation matrix for cell number across the 12 cell types reveals only a single strong correlation, between cholinergic amacrine cells in the INL and in the GCL. Those with significant Pearson correlation coefficients ($p < 0.05$) are emboldened.

rod bipolar cells). Such variation in heritability is largely due to the relative magnitude of the strain differences for these cell types, rather than to any differences in average CoV between the cell types.

Minimal Covariation Exists between Cell Types

Because of the conspicuous variation in cell number across the strains, we searched for correlations between the different cell types; surprisingly, little covariation was found between most cell types (Figure 2). We looked first at developmentally related cell types (i.e., subtypes of the major divisions of retinal nerve cell classes), failing to find significant correlations between the two major classes of photoreceptor, between the three types of cone bipolar cell, or between most comparisons of different amacrine cell subtypes. Likewise, synaptically connected cell types defining the radial pathways through the retina showed no significant correlations, between rods and rod bipolar cells (e.g., Figure 2A), between rod bipolar cells and AII amacrine cells, or between cones and any of the three cone bipolar cells (e.g., Figure 2B). A few cell types did show modest positive correlations (Figure 2C), with coefficients around 0.5, for example, between the rod bipolar cells and the type 2 cone bipolar cells ($r = 0.52$), or between the rods and the type 4 cone bipolar cells ($r = 0.57$). A single exception was found for the two types of cholinergic amacrine cell in the retina, positioned on opposite sides of the inner synaptic layer within the retina and subserving distinct processing of ON versus OFF pathways. These two cell types are not synaptically connected, but they are intimately related developmentally, and their numbers are highly correlated across the strains ($r = 0.81$). Their uniquely high correlation would suggest that none of the other cell types are as tightly related developmentally; indeed, the differentiation of these two cell types is thought to arise secondarily from within the same precursor population during early development (Kim et al., 2000), with each being directed to settle within one of the two nuclear layers, rather than being stipulated cell intrinsically through distinct differentiation pathways, as for instance is assumed for the different types of cone bipolar cell (Strettoi et al., 2010; Xiang, 2013). They confirm the sufficiency of a data set of 30 strains for detecting strong correlations, and although greater numbers of strains might elevate some of the lesser correlation coefficients to significance, the fact remains that no other comparison comes close to this single strong positive correlation, and not a one of them suggests a negative correlation.

Large-Effect QTLs Are Identified for Nearly Every Cell Type

Variation in cell number mapped to one or more independent loci for nearly every cell type (Figure 1C). For example, a quantitative-trait locus (QTL) for rod photoreceptor number was identified proximally on chromosome (Chr) 11 at 11.07 Mb (near rs3023249), with two *B* alleles contributing 495,000 cells, being nearly one-quarter of the range across all strains (Figure 3D). Variation in VGluT3-positive amacrine cells, in comparison, mapped a QTL to the distal end of Chr 5 at 145.20 Mb (rs3696754), although in this case, the presence of *A* alleles at this locus correlated with an increase in cell number, contributing 1,590 cells, or 36% of the difference across the strains (Figure 3C). For all but one cell type examined, one or more loci were identified, and the single largest locus for each type accounted for between 20% and 40% of the range observed across the strains (Figure 1C).

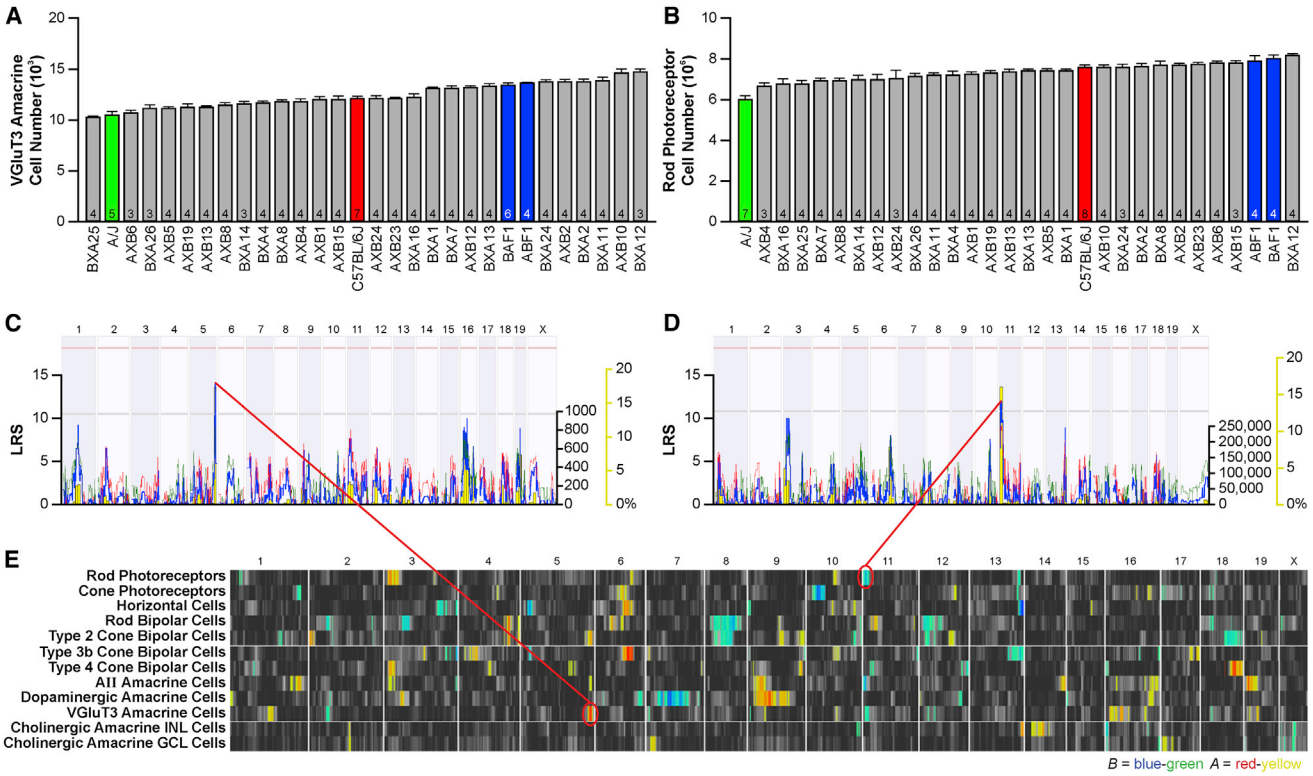

Figure 3. Strain Variation for Each Cell Type Maps Largely to Independent Genomic Loci

(A and B) Variation in VGluT3 amacrine cell number (A) and rod photoreceptor number (B) across the 30 strains. Data shown indicate mean ± SEM and n is number of retinas analyzed.

(C and D) The variation in VGluT3 amacrine cell number mapped to a locus on Chr 5 (C), where *A* alleles correlated with an increase in cell number. Variation in rod photoreceptor number mapped to a locus on Chr 11 (D), where *B* alleles correlated with an increase in rod number.

(E) QTL heatmaps derived from LRS scores using marker regression showed multiple QTL for many of the cell types. Blue-green regions indicate loci where the presence of *B* alleles correlate with an increase in trait values, whereas red-yellow regions indicate loci where *A* alleles correlate with an increase in trait values. Large-effect QTL (summarized in Figure 1C) are mapped for all but one cell type, and multiple QTL are often mapped for some cell types, but variation between cell types rarely maps to the same genomic locus.

Variation between the Cell Types Maps to Independent Genomic Loci

Just as very few of the individual cell types covaried with one another, so too was there minimal evidence for genetic coregulation of cell number. Each of the QTLs identified appears to modulate primarily that cell type, with little evidence of variation in two or more cell types mapping to the same locus (Figure 3E). Some of the modest correlations detected (Figure 2C) occasionally mapped to coincident (and lesser) loci, suggesting some limited genetic coregulation between these cell types (for instance, between rod bipolar cells and type 2 cone bipolar cells, on Chr 4 and Chr 12). Clearly, the variation in cell number identified across cell types cannot be explained by a master variant that modulates proliferation. For example, although retinal area showed slight and heritable variation across the strains that mapped a QTL on Chr 18, this locus did not coincide with any of the loci identified for cell type. A few cell types showed modest correlations with retinal area, the largest being rod photoreceptors (r = 0.53), but the variation in rod number was more substantially dependent upon rod density (r = 0.71). Overall, the variation in retinal cell number arises from genetic variants modulating cell types independent of each other, and independent of retinal area.

Variation in Pre- and Postsynaptic Cell Number Modulates Dendritic Differentiation

Such variation between the sizes of pre- and postsynaptic populations (e.g., Figure 2A) may affect their differentiation. We examined the morphology of the rod bipolar cells in two of the strains of mice, the A/J and F1 strains (Figures 4A and 4B), with the latter containing 16% more rod bipolar cells (Figure 4C). Although soma size was not different between them (Figure 4D), the dendritic field areas of the F1 strain were significantly smaller than those in the A/J strain (Figure 4E), as were the areas of the axonal arbors (Figure 4F). Curiously, the total number of dendritic terminal endings within these narrower F1 dendritic fields was slightly but significantly larger (Figure 4G), suggesting the presence of a larger number of rod photoreceptors afferent to these rod bipolar cells, borne out by the estimates of total rod photoreceptor number in these two strains (Figure 3B), and consistent with the presence of a thicker outer plexiform layer (OPL) containing a distribution of labeled synaptic ribbons that

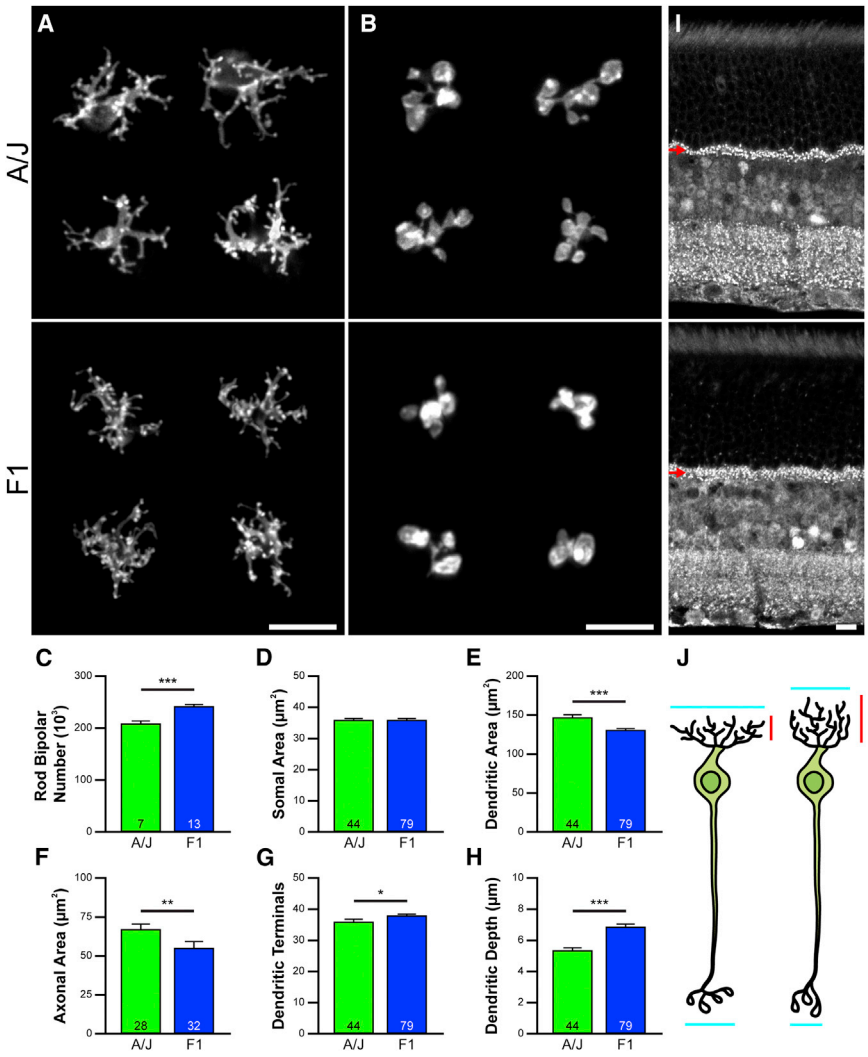

Figure 4. Variation in Pre- and Postsynaptic Cell Number Modulates Dendritic Differentiation

(A–C) Rod bipolar cell dendritic (A) and axonal arbors (B) differ in area in A/J and F1 strains, with the latter strain having 16% more rod bipolar cells than the former strain (C).

(D–F) Soma areas do not differ (D), but dendritic field area (E) and axonal arbor area (F) are each larger in the A/J strain. (G) Despite their smaller dendritic areas, the rod bipolar cells in the F1 strain have significantly more dendritic terminals. (H and I) The F1 strain has a substantially larger rod photoreceptor population (Figure 3B), distributing their presynaptic terminals (labeled with an antibody to CtBP2) across a greater depth of the OPL (I, arrows). The dendritic arbors of their rod bipolar cells are themselves distributed across a greater depth of the OPL (H).

(J) Local homotypic cell density, therefore, constrains dendritic field extent (blue), whereas local afferent density drives terminal formation and distribution within that field area (red).

Scale bars, 10 μm.

Data shown indicate mean ± SEM, and n is the number of retinas analyzed for (C) and the number of cells analyzed for (D)–(H). *$p < 0.05$, **$p < 0.01$, and ***$p < 0.001$.

spanned a greater depth (Figure 4I, arrows). The larger numbers of dendritic terminals formed by those rod bipolar cell dendrites in the F1 strain (Figure 4G) were likewise distributed across a greater depth of the OPL (Figure 4H). Rod bipolar cells, consequently, have their dendritic and axonal arbor growth constrained by the local density of homotypic neighbors, whereas their dendritic depth and number of terminal endings are driven by the density of afferents within their dendritic field (Figure 4J, indicated by the blue and red segments, respectively).

DISCUSSION

We have demonstrated that the number of neurons within a retinal population is precisely specified. This level of specification is comparable across populations showing a 1,000-fold variation in their number, regardless of whether they are packed side by side, form sparse yet regular mosaics, or approach a random distribution. Cell number is, however, a complex trait controlled by multiple genetic variants, made clear by the graded yet substantial within-class variation in total number across the different strains of mice, for every cell type.

This large variation in cell number present across the RI strains was mapped to genomic loci for all but one of the cell types investigated, but rarely did that variation map to the same chromosomal loci. Variation in cell number, therefore, reflects the actions of multiple variants affecting the final numbers of each cell type largely independent of one another. This lack of genetic coregulation is manifest in the largely uncorrelated variation between different pairs of neuron types. Hence, although certain cell types are known to share transcriptional regulatory control during their development (Bassett and Wallace, 2012; Ohsawa and Kageyama, 2008), variants in these genes appear not to be major codeterminants of the variation in cell number in maturity.

These results do not, of course, prove the negative, that genomic coregulation does not contribute to the determination of retinal cell number. First, it remains possible that allelic variants in genes contributing small-to-modest effect size for multiple cell types have gone undetected due to an insufficient fractioning of the genome with only 26 RI strains. And second, there may be allelic variants in genes contributing large and common effects in various cell classes, but these may not differ between the parental genomes examined in the present study. Our data simply indicate that the genetic variation discriminating these two parental strains has a far greater influence on the variation in the numbers of individual cell types, rather than on covariation between the cell types.

In addition to such lack of covariation among developmentally related cell types, synaptically connected cell types also failed to

show significant covariation in their numbers, consistent with other studies showing a lack of spatial correlation between them (Rockhill et al., 2000). Differentiation programs, however, while directing cell-type-specific dendritic patterning and outgrowth, may also equip neurons to modulate their morphogenesis in response to varying homotypic and afferent densities. Such developmental plasticity enables two populations of synaptically connected neurons, the numbers of which vary widely and largely independent of one another, to conserve a fundamental design feature: a uniform dendritic coverage by the postsynaptic cell to sample the entirety of the population of their afferents. Curiously, this plasticity would appear to be the rule in the OPL (Lee et al., 2011; Reese et al., 2005), whereas within the inner plexiform layer, there are multiple exceptions to it (Farajian et al., 2004; Keeley and Reese, 2010a; Lin et al., 2004).

Independent genetic control between populations has now been shown to be present at three different levels of organization within the CNS: first, between interconnected local circuit neurons within a structure (shown here); second, between long-range interconnected populations of projection neurons (Seecharan et al., 2003); and third, between interconnected brain regions (Hager et al., 2012). Collectively, these three levels of independent control argue against strong developmental constraints upon neuron number or brain structure size within species. Natural selection occurs at the behavioral level, and behavior is remarkably well buffered from such enormous variation in cell number through the actions of afferent- and homotypic-dependent plasticity instructing the formation of neuronal circuits (Reese et al., 2011).

EXPERIMENTAL PROCEDURES

Mice

Parental C57BL/6J and A/J strain mice, their reciprocal F1 offspring (B6AF1/J and AB6F1/J), and RI mice of the AXB/BXA strain-set were obtained from the Jackson Laboratory or bred in-house at the Animal Resource Center at University of California, Santa Barbara (UCSB). All RI strain mice were females for the analysis of 11 of the cell types; the cone photoreceptor analysis was the exception, including equal numbers of male and female mice in each strain. All of the parental and F1 mice were of both sexes. Adult mice ~1–3 months of age were heavily anesthetized and then perfused intracardially with 0.9% saline followed by 4% paraformaldehyde in 0.1 M sodium phosphate buffer (pH 7.2 at 20°C). Retinas were dissected and prepared as whole mounts as described previously (Whitney et al., 2009), with extreme care being taken to maintain the entirety of the retina intact. All procedures were conducted under authorization by the Institutional Animal Care and Use Committee at UCSB and conform to the American Veterinary Medical Association Guidelines on Euthanasia.

Labeling of Specific Cell Types

Whole retinas were labeled using standard immunofluorescence procedures, as described previously (Whitney et al., 2009, 2011a). The two retinas from each mouse were each double labeled with different primary antibodies raised in distinct species, enabling multiple cell types to be counted from each mouse. The primary antibodies used included the following: (1) a cocktail of rabbit polyclonal antibodies to red/green and blue cone opsin to label all cone outer segments (each at 1:1,000; Millipore AB5405 and AB5407); (2) a mouse monoclonal antibody to calbindin D-28 to label horizontal cells (1:10,000; Sigma C9848); (3) a rabbit polyclonal antibody to protein kinase C to label rod bipolar cell axons (1:10,000; Cambio CA-1042); (4) a mouse monoclonal antibody to synaptotagmin2 to label the type 2 cone bipolar cell axons (1:100; Zebrafish International Resource Center ZDB-ATB-081002-25); (5) a mouse monoclonal antibody to protein kinase A regulatory subunit IIβ to label type 3b cone bipolar cell dendritic stalks (1:3,000; BD Biosciences 610626); (6) a mouse monoclonal antibody to Calsenilin to label type 4 cone bipolar cells (1:1,000; Millipore 05-756); (7) an affinity-purified rabbit polyclonal antibody to Prox1 to label AII amacrine cells (1:1,000; Covance PRB-238C); (8) a mouse monoclonal antibody to tyrosine hydroxylase to label dopaminergic amacrine cells (1:10,000; Sigma T1299); (9) a guinea pig polyclonal antibody to the VGluT3, to label the population of VGluT3 amacrine cells (1:3,000; Millipore AB5421); and (10) an affinity-purified goat polyclonal antibody to choline acetyltransferase to label cholinergic amacrine cells in the inner nuclear layer (INL) and in the ganglion cell layer (GCL) (1:50; Millipore AB144P). Primary antibodies were subsequently detected using donkey host secondary antibodies to rabbit, mouse, guinea pig, or goat immunoglobulin Gs conjugated to Cy2 or Cy3 (1:200; Jackson ImmunoResearch Laboratories), or to Alexa Fluor 488 or Alexa Fluor 546 (1:200; Life Technologies). Examples of labeled specimens are provided in Figure 1B.

To sample the rod photoreceptor population, the above-mentioned protocol was modified by further fixation of the flattened retina in glutaraldehyde to enhance Nomarski contrast of individual inner segments for subsequent viewing. Retinas were then rinsed and incubated overnight in peanut agglutinin conjugated to Alexa Fluor 488 (PNA-488) (1:200; Life Technologies L21409) to label the sheaths of the cone outer and inner segments to discriminate them from the rods.

Quantification of Cell Number

The methodologies and results for the quantification of cone photoreceptors, horizontal cells, and dopaminergic amacrine cells have previously been published (Whitney et al., 2009, 2011a, 2011b). Fields containing rod photoreceptor inner segments were imaged using a 60× oil immersion objective on a Nikon FXA fluorescence photomicroscope and an Olympus DP11 digital camera, with each field being imaged twice: first, using differential interference contrast optics to discriminate individual inner segments; and second, under fluorescence to detect PNA-positive profiles (cones). The latter counts were then subtracted from the former to determine rod number per field. Each retina was sampled multiple times in a 1 mm square grid (average of 14 samples per retina), sampling a field size of 225 μm^2 at each location.

For all other cell types, each retinal quadrant was sampled, either at a mid-eccentric location, or at both a peripheral and central location. Retinas were sampled using an Olympus microscope equipped with a Sony video camera and linked to a computer running Bioquant Nova Prime (R&M Biometrics), sampling field sizes of approximately 16,000 μm^2 for rod bipolar cells and type 4 bipolar cells; 32,000 μm^2 for type 2 bipolar cells, type 3b bipolar cells, and AII amacrine cells; 60,000 μm^2 for the cholinergic amacrine cells; and 175,000 μm^2 for VGluT3 amacrine cells. For the cholinergic amacrine cells, images were collected at two depths in the retina, sampling from the INL and GCL independently.

The outline of each retina was subsequently measured using Bioquant Nova Prime. Retinal area was multiplied by average cell density to estimate the total number of cells per retina. Three to four retinas were routinely counted in every RI and F1 strain for each cell type, with three exceptions where we could only obtain an n of two mice at the time of sampling a particular cell type. Parental strains were frequently sampled in larger numbers, averaging around seven retinas for each cell type. For a few cell types, one or two strains were unavailable at the time of sampling for those types, so the analysis for those cell types was conducted with only 25 or 24 RI strains.

All counting was done by eye (i.e., without automated image analysis to extract labeled profiles), marking individual profiles on the screen to ensure no double-counting within a field. As a further assurance against bias in the process of counting, particularly for the more densely packed cell types (i.e., the rod photoreceptor population, all four bipolar cell populations, and the AII amacrine cell population), as well as for the VGluT3 population, counting for these cell types was conducted "blind" to strain, with mice of different strains being randomly intermingled.

Calculating Heritability

Heritability was estimated by computing the ratio $(0.5 \times X)/((0.5 \times X) + Y)$, where X is variance(strain) and Y is variance(error). Only the RI strains have

been included in the calculation of heritability (Hegmann and Possidente, 1981).

QTL Mapping

QTL mapping was performed using the mapping module available at GeneNetwork (http://www.genenetwork.org). Only the RI strain data were included in this mapping. Every RI strain has a unique mix of *A* and *B* haplotypes across every chromosome (with the exceptions of the Y chromosome and the mitochondrial genome) due to the nearly random recombination events occurring in the course of inbreeding different pairs of F2 siblings (Williams et al., 2001). QTL mapping estimates the genetic control of a trait with the variation of *A* versus *B* alleles throughout the genome. GeneNetwork implements simple and composite interval mapping for each trait and estimates the genome-wide p value of a type I error by permutation. It also generates "heatmaps" for each trait that enable easy comparisons between multiple traits, although in this case using marker regression rather than interval mapping. These heatmaps identify any locus with a likelihood ratio statistic (LRS) score greater than 0.5 of the suggestive LRS threshold, climbing to a maximum (for each cell type) set by the significant LRS threshold for that cell type (indicated by blue-green or red-orange in Figure 3E). This liberal criterion maximizes the likelihood of detecting lesser QTLs that individually might not garner attention, but if reinforced across multiple cell types, should draw further scrutiny. The suggestive ($p = 0.67$) and significant ($p = 0.05$) LRS thresholds are computed for each cell type individually, based on 1,000 random permutations of the strain data for that cell type (indicated by the horizontal gray and pink lines in Figures 3C and 3D). The suggestive threshold was used as the minimal criterion for defining a mapped QTL in Figure 1C. The primary cell type data (means and SEMs) have been permanently deposited in GeneNetwork, with their phenotype accession identifiers for the mouse AXB/BXA Published Phenotypes database being indicated in Figure 1C.

Morphometric Analysis of Dendritic Morphology

Individual rod bipolar cells in the A/J and F1 strains were injected with DiI to study their morphology. Because rod photoreceptor and rod bipolar cell number were comparable between the BAF1 and ABF1 strains, their data have been combined here for comparison with the A/J strain. All procedures for labeling and analysis have been described previously (Keeley and Reese, 2010b). Comparisons of rod bipolar cell morphology were tested for statistical significance using Student's t tests.

ACCESSION NUMBERS

Of the accession numbers listed in Figure 1C, three (Cone, HC, and DA) were published previously (Whitney et al., 2009, 2011a, 2011b). The following were recently deposited in the AXB/BXA Published Phenotypes database on GeneNetwork (http://www.genenetwork.org) in association with this work: 10268 (Rod), 10202 (RBC), 10181 (CBC2), 10257 (CBC3b), 10263 (CBC4), 10179 (All), 10262 (VGluT3), 10131 (ChAT INL), and 10129 (ChAT GCL).

SUPPLEMENTAL INFORMATION

Supplemental Information includes one table and can be found with this article online at http://dx.doi.org/10.1016/j.devcel.2014.05.003.

ACKNOWLEDGMENTS

This research was supported by the National Institutes of Health (EY-019968; RR-022585).

Received: December 16, 2013
Revised: March 21, 2014
Accepted: May 2, 2014
Published: June 19, 2014

REFERENCES

Balasubramanian, V., and Sterling, P. (2009). Receptive fields and functional architecture in the retina. J. Physiol. *587*, 2753–2767.

Bassett, E.A., and Wallace, V.A. (2012). Cell fate determination in the vertebrate retina. Trends Neurosci. *35*, 565–573.

Farajian, R., Raven, M.A., Cusato, K., and Reese, B.E. (2004). Cellular positioning and dendritic field size of cholinergic amacrine cells are impervious to early ablation of neighboring cells in the mouse retina. Vis. Neurosci. *21*, 13–22.

Hager, R., Lu, L., Rosen, G.D., and Williams, R.W. (2012). Genetic architecture supports mosaic brain evolution and independent brain-body size regulation. Nat. Commun. *3*, 1079.

Hegmann, J.P., and Possidente, B. (1981). Estimating genetic correlations from inbred strains. Behav. Genet. *11*, 103–114.

Keeley, P.W., and Reese, B.E. (2010a). Morphology of dopaminergic amacrine cells in the mouse retina: independence from homotypic interactions. J. Comp. Neurol. *518*, 1220–1231.

Keeley, P.W., and Reese, B.E. (2010b). Role of afferents in the differentiation of bipolar cells in the mouse retina. J. Neurosci. *30*, 1677–1685.

Kim, I.-B., Lee, E.-J., Kim, M.-K., Park, D.-K., and Chun, M.-H. (2000). Choline acetyltransferase-immunoreactive neurons in the developing rat retina. J. Comp. Neurol. *427*, 604–616.

Lee, S.C., Cowgill, E.J., Al-Nabulsi, A., Quinn, E.J., Evans, S.M., and Reese, B.E. (2011). Homotypic regulation of neuronal morphology and connectivity in the mouse retina. J. Neurosci. *31*, 14126–14133.

Lin, B., Wang, S.W., and Masland, R.H. (2004). Retinal ganglion cell type, size, and spacing can be specified independent of homotypic dendritic contacts. Neuron *43*, 475–485.

Lui, J.H., Hansen, D.V., and Kriegstein, A.R. (2011). Development and evolution of the human neocortex. Cell *146*, 18–36.

Ohsawa, R., and Kageyama, R. (2008). Regulation of retinal cell fate specification by multiple transcription factors. Brain Res. *1192*, 90–98.

Reese, B.E., Raven, M.A., and Stagg, S.B. (2005). Afferents and homotypic neighbors regulate horizontal cell morphology, connectivity, and retinal coverage. J. Neurosci. *25*, 2167–2175.

Reese, B.E., Keeley, P.W., Lee, S.C., and Whitney, I.E. (2011). Developmental plasticity of dendritic morphology and the establishment of coverage and connectivity in the outer retina. Dev. Neurobiol. *71*, 1273–1285.

Rockhill, R.L., Euler, T., and Masland, R.H. (2000). Spatial order within but not between types of retinal neurons. Proc. Natl. Acad. Sci. USA *97*, 2303–2307.

Seecharan, D.J., Kulkarni, A.L., Lu, L., Rosen, G.D., and Williams, R.W. (2003). Genetic control of interconnected neuronal populations in the mouse primary visual system. J. Neurosci. *23*, 11178–11188.

Southwell, D.G., Paredes, M.F., Galvao, R.P., Jones, D.L., Froemke, R.C., Sebe, J.Y., Alfaro-Cervello, C., Tang, Y., Garcia-Verdugo, J.M., Rubenstein, J.L., et al. (2012). Intrinsically determined cell death of developing cortical interneurons. Nature *491*, 109–113.

Strettoi, E., Novelli, E., Mazzoni, F., Barone, I., and Damiani, D. (2010). Complexity of retinal cone bipolar cells. Prog. Retin. Eye Res. *29*, 272–283.

Whitney, I.E., Raven, M.A., Ciobanu, D.C., Williams, R.W., and Reese, B.E. (2009). Multiple genes on chromosome 7 regulate dopaminergic amacrine cell number in the mouse retina. Invest. Ophthalmol. Vis. Sci. *50*, 1996–2003.

Whitney, I.E., Raven, M.A., Ciobanu, D.C., Poché, R.A., Ding, Q., Elshatory, Y., Gan, L., Williams, R.W., and Reese, B.E. (2011a). Genetic modulation of horizontal cell number in the mouse retina. Proc. Natl. Acad. Sci. USA *108*, 9697–9702.

Whitney, I.E., Raven, M.A., Lu, L., Williams, R.W., and Reese, B.E. (2011b). A QTL on chromosome 10 modulates cone photoreceptor number in the mouse retina. Invest. Ophthalmol. Vis. Sci. *52*, 3228–3236.

Williams, R.W., Gu, J., Qi, S., and Lu, L. (2001). The genetic structure of recombinant inbred mice: high-resolution consensus maps for complex trait analysis. Genome Biol. *2*, RESEARCH0046.

Xiang, M. (2013). Intrinsic control of mammalian retinogenesis. Cell. Mol. Life Sci. *70*, 2519–2532.

Xiong, M., and Finlay, B.L. (1996). What do developmental mapping rules optimize? Prog. Brain Res. *112*, 351–361.